Aerosol Science and Technology

ISSN: 0278-6826 (Print) 1521-7388 (Online) Journal homepage: www.tandfonline.com/journals/uast20

Role of mucin in controlling evaporation and hygroscopic behavior of human respiratory droplets and potential implications for spreading of pathogens

Yue Meng, Alexei Kiselev, Denis Duft, Thomas Dresch & Thomas Leisner

To cite this article: Yue Meng, Alexei Kiselev, Denis Duft, Thomas Dresch & Thomas Leisner (27 May 2025): Role of mucin in controlling evaporation and hygroscopic behavior of human respiratory droplets and potential implications for spreading of pathogens, Aerosol Science and Technology, DOI: 10.1080/02786826.2025.2505036

To link to this article: https://doi.org/10.1080/02786826.2025.2505036

AEROSOL SCIENCE AND TECHNOLOGY
https://doi.org/10.1080/02786826.2025.2505036

Role of mucin in controlling evaporation and hygroscopic behavior of human respiratory droplets and potential implications for spreading of pathogens

Yue Meng[a], Alexei Kiselev[a], Denis Duft[a], Thomas Dresch[a], and Thomas Leisner[a,b]

[a]Karlsruhe Institute of Technology, Institute of Meteorology and Climate Research, Karlsruhe, Germany; [b]University of Heidelberg, Institute of Environmental Physics, Heidelberg, Germany

ABSTRACT

The transmission of respiratory pathogens through aerosolized expiratory secretions, in the form of droplets and aerosols, represents a primary route for the spreading of infectious respiratory diseases, including COVID-19. Investigating the droplet micro-environment occurring under different conditions to understand the infectivity of pathogens carried by droplets holds significant implications for controlling the dissemination of airborne diseases. Here, we conducted measurements of the evaporation and hygroscopic growth of levitated artificial human saliva droplets using an electrodynamic balance. These measurements were complemented with the characterization of the morphology of evaporated droplet residuals using a scanning electron microscope and light scattering patterns, providing a further understanding of the underlying mechanisms of the relative humidity-dependent inactivation of viruses. Results showed that saliva droplets exhibited a complex morphology change behavior during evaporation at RH below 45%. The presence of mucin slightly retarded the evaporation rate and significantly impeded the water uptake process of saliva droplets. This phenomenon was attributed to the possible formation of a mucin-enriched layer on the surface of the saliva droplets during the evaporation process. These findings emphasize the significant role of mucin in affecting the properties of saliva droplets during evaporation and rehydration, thereby potentially influencing the persistence of pathogens.

GRAPHICAL ABSTRACT

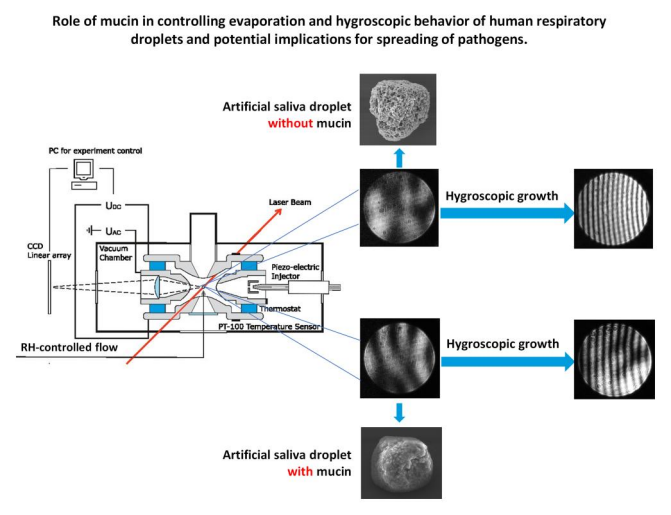

ARTICLE HISTORY

Received 6 November 2024
Accepted 29 April 2025

EDITOR

Cari Dutcher

CONTACT Yue Meng yue.meng@kit.edu Institute of Meteorology and Climate Research, Karlsruhe Institute of Technology, Karlsruhe 76021, Germany.

Supplemental data for this article can be accessed online at https://doi.org/10.1080/02786826.2025.2505036.

1. Introduction

Infectious respiratory diseases, such as coronavirus disease 2019 (COVID-19), severe acute respiratory syndrome (SARS), Middle East respiratory syndrome (MERS), influenza and measles, impose a significant global public health burden, resulting in millions of deaths annually (Kudo et al. 2019; Wang et al. 2021; Niazi et al. 2021a). Airborne transmission is now widely recognized as one of the main routes for the spread of numerous respiratory viruses (Morawska and Cao 2020; Prather, Wang, and Schooley 2020; Wang et al. 2021; Lewis 2022). Pathogenic microorganisms, including viruses and bacteria that can infect the respiratory system, are commonly disseminated through aerosolized expiratory secretions, such as mucus and saliva, in the form of aerosols (<5 μm in diameter) and droplets (>5–100 μm), when an infected individual breathes, coughs, sneezes, talks, or laughs (Liu et al. 2017; Ahlawat, Wiedensohler, and Mishra 2020; Morawska and Cao 2020; Tang et al. 2021; Wang et al. 2021; Oswin et al. 2022). Aerosols and droplets laden with viruses, suspended in the air for extended periods of time, inevitably pose a risk to human health. However, a deeper understanding of how physicochemical properties of exhaled aerosols and droplets are related to the infectivity of viruses is still limited, despite its critical importance in mitigating the airborne transmission of diseases.

Keeping pathogenic microorganisms viable is a crucial prerequisite for initiating infection (Huynh et al. 2022). The viability of pathogens is linked to environmental factors such as temperature, humidity, sunlight, and pH (Lin, Schulte, and Marr 2020; Schuit et al. 2020; Smither et al. 2020; Guo et al. 2021; Niazi et al. 2021a; Luo et al. 2023). Numerous studies have demonstrated that relative humidity (RH) plays a multifaceted role in determining the survival of viruses in droplets (Prussin et al. 2018; Lin and Marr 2020; Niazi et al. 2021b). Lin and Marr (2020) reported that viruses preserve their activity at RH below 40% and near 100%, but become less active at intermediate RH, showing a distinctive U-shaped, RH-dependent infectivity pattern. This unique U-shaped pattern has been observed in many airborne viruses, including severe acute respiratory syndrome coronavirus 2 (SARS-CoV-2) and influenza A (Yang, Elankumaran, and Marr 2012; Lin, Schulte, and Marr 2020; Niazi et al. 2021a). The reason for the RH-dependent pattern in virus infectivity in droplets is less clear, but several factors have been suggested. On the one hand, low RH negatively affects the immune system's ability to respond to pathogenic microorganisms, leading to a higher risk of infection (Kudo et al. 2019; Ahlawat, Wiedensohler, and Mishra 2020). On the other hand, changes in the physicochemical properties of exhaled respiratory droplets under different RH conditions may also be responsible (Huynh et al. 2022).

Respiratory droplets, which contain water, various salts, proteins, and lipids (Boat and Cheng 1980), experience physicochemical changes during the evaporation as being exhaled from the respiratory tract (close to 100% RH) into the ambient environment (typically ranging from 30% to 60% RH). The evaporation process results in the loss of water, leading to size reduction, increased solute concentrations, and changes in phase, morphology, viscosity and pH (Walker et al. 2021; Oswin et al. 2022; Luo et al. 2023). Previous research has suggested that when saliva droplets are exposed to low RH, the rapid crystallization of salts could protect viruses from prolonged exposure to a highly concentrated saline solution (Niazi et al. 2021b). However, other studies have suggested that efflorescence is suppressed due to the formation of an organic amorphous shell, formed by proteins and lipids at the later stage of droplet drying (Stewart et al. 2015; Huynh et al. 2022).

Mucins are complex glycoproteins found in human saliva and play a crucial role in maintaining oral health and forming a protective barrier on the surfaces of the oral cavity (Ali et al. 2011; Corfield 2015). They make up a significant portion of the total protein content in saliva, even though the exact concentration can vary among individuals and is influenced by factors such as hydration, overall health and oral diseases. Two major mucins found in human saliva, produced from respiratory tract, are designated as MUC5B and MUC7 (Takehara et al. 2013). MUC5B is a larger mucin protein compared to MUC7, and it is responsible for the gel-like properties of saliva. MUC7, existing primarily as monomers or dimers, is involved in maintaining the fluidity and lubrication properties of saliva by preventing it from becoming too viscous, thereby contributing to physiological functions such as speaking, chewing, and swallowing (Corfield 2015). Considering the properties and significant content of mucin, it may play a role in the physicochemical alteration of saliva droplets, thereby affecting the activity of pathogens. Alexander et al. (2022) reported that mucin in the evaporating respiratory aerosol transiently sustains the coronavirus infectivity by enhancing the formation of "protective inclusions," which appear to protect viruses from inactivation. Mucin is also thought to influence

evaporation and hygroscopic growth of exhaled respiratory droplets. Tian et al. (2024) compared the evaporation of artificial saliva droplets containing mucin and droplets containing all other solutes except mucin and found only marginal difference in evaporation rate at 40% RH. In their study, they observed a small delay in crystallization times of mucin-containing droplets. Based on this observation, they hypothesized that mucin may form a viscous surface film that affects mass transport and crystallization dynamics, resulting in a different amount of residual water that may be kinetically limited in release (Tian et al. 2024). Thus, a clear and detailed understanding of the role of mucin in the evaporation of respiratory droplets is essential for elucidating RH-dependent virus activity.

When dried saliva particles enter a region of high RH, they can undergo hygroscopic growth. This process is critical to investigate as it can impact droplet size, density, composition and residence time in a suspended state, as well as the lung penetration depth upon inhalation, which has significant implications for the potential airborne transmission and infectivity of viruses. The primary factors governing hygroscopic growth are composition and morphology of droplets, along with the ambient RH (Chen et al. 2021; Vu, Shi, and Harrison 2021). Droplets exhibiting higher hygroscopicity may grow to larger sizes and settle more rapidly, while less hygroscopic particles may stay suspended in the surrounding air for longer periods.

Moreover, saliva droplets can be influenced by the uptake of water vapor and other ambient gases from the environment. The pH of saliva is typically close to neutral, around 6.2–7.6 (Baliga, Muglikar, and Kale 2013). Exhaled saliva droplets exhibit an increase in pH to a highly alkaline level, approximately 10, attributed to the loss of bicarbonate from droplets which is converted to $CO_{2(g)}$ (Haddrell et al. 2023). The change of pH within the saliva droplets also plays an important role in the loss of viral infectivity. Luo et al. (2023) investigated the role of aerosol acidity in the inactivation of SARS-CoV-2 in indoor environment and reported that SARS-CoV-2 maintained their infectivity down to a pH of 3. A notably shorter inactivation time for SARS-CoV-2 was predicted in the acidified indoor air with pH < 3. It was also suggested that the presence of mucus provides some protection against inactivation below pH of 3. Oswin et al. (2022) demonstrated that the stability of the virus could be increased by elevating the CO_2 content in the air, a result of CO_2 buffering the alkaline droplets. It is important to note that the pH change during the water uptake process is influenced by the initial composition of the droplet. Given the chemical complexity of saliva droplets, a quantitative description of their hygroscopic growth is missing so far.

The state of the respiratory particles (liquid, semi-solid or solid) may influence their resuspension from surfaces after initial sedimentation. As shown recently (Nikfar et al. 2021), liquid droplets as large as 200 µm can be resuspended from partly wettable surfaces as a result of normal human activities. For droplets on non-wettable surfaces or semi-dry residual particles, the resuspension could be achieved for smaller particle sizes and lower detachment velocities. Clearly, knowledge of the respiratory particle phase state at the moment of sedimentation would allow accessing the probability of the particle resuspension and would thus lead to better understanding of air-transmitted infectious diseases.

In this study, we investigated the influence of mucin on the evaporation and hygroscopic growth of artificial saliva droplets by levitating single saliva droplets in an electrodynamic balance (EDB) at RH ranging from <5% to 97%. Additionally, we provided a comprehensive analysis of the microstructure and morphology of artificial saliva droplets in their equilibrium state using a scanning electron microscope (SEM). Our findings contribute to understanding the factors controlling the RH-dependent infectivity of viruses contained in respiratory droplets.

2. Experiment

2.1. Artificial saliva formulation

Two types of artificial saliva were investigated in this study: artificial saliva with mucin (ASM, pH = 7.0, catalog No. 1700–0316, Pickering Laboratories, Inc., Mountain View, USA; mucin [from porcine stomach] type II) and artificial saliva without mucin (AS, pH = 7.1). The AS was prepared using the same components as in the ready-to-use ASM, excluding the mucin. The detailed compositions of the artificial saliva solutions are shown in Table 1. Since the commercial ASM was stabilized with Pro-clean (a preservative) to prevent bacterial growth, the laboratory-prepared AS contained an equal amount of Pro-clean in our study. The composition of Pro-clean is shown in the online supplementary information (SI) Table S1. The stock solutions of both artificial saliva formulations were diluted to 20% *v/v* with deionized water to prevent clogging of the droplet-on-demand dispenser.

Table 1. Compositions of artificial saliva with mucin (ASM) and without mucin (AS).

ASM	Concentration [g/L]	AS	Concentration [g/L]
NaCl	0.88	NaCl	0.88
$NaHCO_3$	0.42	$NaHCO_3$	0.42
KH_2PO_4	0.2096	KH_2PO_4	0.2096
K_2HPO_4	0.4285	K_2HPO_4	0.4285
KCl	1.04	KCl	1.04
KSCN	0.19	KSCN	0.19
$CaCl_2{\cdot}H_2O$	0.13	$CaCl_2{\cdot}H_2O$	0.13
$MgCl_2{\cdot}7H_2O$	0.04	$MgCl_2{\cdot}6H_2O$	0.0368
NH_4Cl	0.11	NH_4Cl	0.11
Urea	0.12	Urea	0.12
Mucin	3.0	Pro-clean	0.3 mL/L
Pro-clean	0.3 mL/L		

2.2. Measurements of evaporation and hygroscopic growth of artificial saliva droplets

2.2.1. Experimental setup

The evaporation and hygroscopic growth of artificial saliva droplets were measured using an EDB system, which allows for the levitation of a single, charged droplet exposed to a laminar flow of humidified synthetic air. The operation principle has been comprehensively described in previous studies (Rzesanke et al. 2012; Hoffmann et al. 2013). Briefly, an Alternating Current (AC) potential was applied to the torus electrode of the EDB to levitate individual droplets, and a Direct Current (DC) potential was applied to the top and bottom electrodes to offset the gravitational force and the drag force acting on the droplet, thereby maintaining the droplet levitating in the center of the trap. In this study, the RH-controlled synthetic air flow was directed through the EDB from below at a flow rate of 0.07 sL/min.

Droplets with an initial radius of (48 ± 2) µm were generated using a piezoelectric drop-on-demand dispenser (GeSIM model SPIP: A010-006, with a cylindrical housing). The droplets were inductively charged to approximately − 0.8 pC by applying a + 300 V voltage to a ring electrode placed in front of the dispenser tip. A single droplet was stably levitated in the center of the trap, while exposed to a laminar airflow with RH ranging from <5% to 97%. The RH was monitored by a humidity sensor (Sensirion SHT41) positioned in the airflow, with an accuracy of ± 1.5% RH. The temperature inside the trap was maintained at a constant (17.8 ± 0.3)°C using a thermostat (Julabo USA, Inc.).

The levitated droplet was illuminated with a 632.8 nm 25 mW HeNe laser. To determine the droplet position, scattered light was detected by a vertically oriented linear Charge-Coupled Device (CCD) detector (Spectronics Devices). To calculate the size and to infer the shape of artificial saliva droplets, the two-dimensional light scattering pattern within the solid angle 18.8° centered around 45° scattering angle was recorded once a second using a CCD camera (model DMK21BF04, ImagingSource). The size of the droplet was determined by comparing the recorded light scattering patterns with the theoretical scattering phase function. This function was calculated by assuming a refractive index of droplets changing from $n = 1.333$, which corresponds to the initial concentration of 20% *v/v* diluted artificial saliva (primarily water), to a maximum of $n = 1.5$ for dry residual particles. The refractive index of $n = 1.5$ was chosen based on commonly accepted refractive indexes of the organic and inorganic components typically found in saliva residues (Ebert et al. 2002). The relative uncertainty of the measured radius was estimated to be 2.2%. A detailed description of the size measurement method using light scattering patterns is provided in a previous study (Singh et al. 2023).

2.2.2. Evaporation and hygroscopic growth measurements

Droplets were introduced into the trap after both RH and temperature have been kept at set values for 30 min. The hygroscopic growth experiments were conducted by increasing RH of the gas flow from low levels to 97%. Initially, droplets were injected and stably levitated under specific RH conditions (<5%, 15%, 30%, 45%, 60%, and 75% RH) for a duration of 5 min. Subsequently, the RH in the trap was raised to 97%, with no impact on the stable levitation of droplets. The timescale for the trap to adjust to the new RH setting varied depending on the initial RH, typically ranging from three to ten minutes. The droplets remained levitated for an additional hour after reaching and stabilizing at 97% RH. Light scattering images were continuously recorded from the beginning to the end of the experiments.

2.3. Scanning electron microscope (SEM) study

Artificial saliva droplets, which had reached an equilibrium size under well-defined RH conditions, were deposited onto a 2 mm x 2 mm silicon wafer, as described in Hoffmann et al. (2013). Then, the extracted samples were placed into an airtight container under low-humidity conditions (<2% RH at room temperature) and transferred to the electron microscope. The transfer protocol ensured that the droplets collected on a Si-wafer would not be exposed to humid air. The Si-wafers were observed in the

Environmental Scanning Electron Microscope (ESEM, FEI Thermo Fisher Quattro S) at 50 Pa N_2 as the background gas, avoiding the sputter-coating under high vacuum and thus preserving the morphology of the samples.

3. Results and discussion

3.1. Evaporation behavior of levitated saliva droplets

The evaporation behavior of levitated artificial saliva droplets, both with and without mucin, was examined at a constant temperature of (17.8 ± 0.3)°C and under 7 different RH values ranging from <5% to 97%, as shown in Figure 1. Single droplets of diluted artificial saliva solution with an initial radius of (48 ± 2) µm were injected into the EDB at fixed RH values. The droplets evaporated until reaching an equilibrium state. We observed that once in equilibrium, the droplets maintained their size without further changes. Here, the droplets were kept in an equilibrium state for a five-minute period. The process was repeated 10 times at each RH value to obtain the statistical average of the equilibrium size.

At the initial stage, the evaporation of the diluted ASM and AS droplets follows a similar pattern. As evaporation continues, the loss of water leads to a reduction of droplet size and an increase of solute concentration. The red dotted line at radius of (28 ± 1) µm in Figure 1 marks the size, at which saliva droplets return to the concentration of the original stock solution, which corresponds to the composition of the representative natural human saliva fluid. Here, we speak of the radius of (28 ± 1) µm as the (stock solution) concentration-equivalent size (R_{ce}).

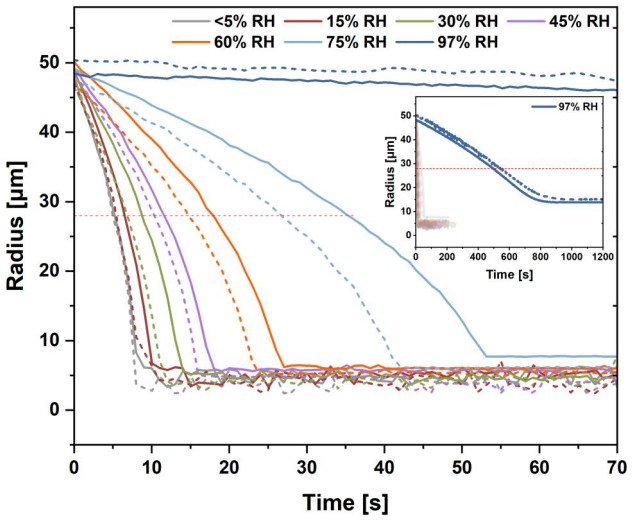

Figure 1. Comparison of the evaporation process of representative artificial saliva droplets containing mucin (ASM, solid lines) and artificial saliva droplets without mucin (AS, dashed lines) under different RH conditions. All measurements were carried out at a temperature of (17.8 ± 0.3)°C. The red dotted line indicates the size of saliva droplets when they reach the concentration of the original stock solution. The complete evaporation process of saliva droplets at 97% RH is shown by a zoom-out view in the inset.

As expected, the evaporation rate of saliva droplets proceeds faster at lower RH. AS droplets evaporate faster and reach equilibrium more quickly than ASM droplets, as shown in Table 2. After the droplets have reached an equilibrium state, they can be levitated without exhibiting any detectable change of size.

The equilibrium size of saliva droplets is a critical parameter in determining the transmissibility of pathogens (Parienta et al. 2011; Marr et al. 2019). It determines how long virus-laden droplets remain suspended in the air before settling on surfaces or the ground, and it also affects how deeply these droplets can penetrate into the respiratory system if inhaled. As shown in Figure 1, the radius of saliva droplets evaporating at humid conditions (RH ≥ 75%) stops at relatively larger equilibrium sizes, while the sizes of saliva droplets that evaporate at intermediate and dry conditions are smaller. Significant fluctuations in equilibrium size are observed in saliva droplets evaporating under dry conditions (RH ≤ 45%). This phenomenon is attributed to the distortion of the light scattering patterns at their equilibrium state, which may be a result of an inhomogeneity and a non-spherical shape of the saliva droplets. The equilibrium size is calculated as the average over all measurements of droplets size at these dry conditions.

Figure 2a shows the average equilibrium size of saliva droplets, obtained from measurements of ten droplets at each RH. The ASM droplets equilibrate at a larger size compared to AS droplets. This difference in equilibrium size can be attributed to two factors: (1) The ASM droplets have an additional 3 g/L of mucin, while the other components remain the same as in the mucin-free saliva droplets. This extra mass contributes directly to the droplet's size at equilibrium. (2) Mucin, a high-molecular-weight glycoprotein, potentially forms a viscous layer that limits water loss, thereby resulting in a larger equilibrium size (see discussion in Section 3.2). The ratio shown in Figure 2b applies for droplets of concentration-equivalent size (R_{ce} = (28 ± 1) µm), at which point the diluted saliva droplets have the concentration of the original stock solution. A slight trend toward larger equilibrium size with increasing RH is observable from RH <5% to 60%, with a ratio R_{eq}/R_{ce} falling within the

Table 2. Time required for artificial saliva droplets to reach the equilibrium state and their equilibrium radius. Listed are average time and standard deviation for ten droplets measured at each setting.

	Time to reach the equilibrium state [s]		Equilibrium radius [μm]	
Relative humidity [%]	ASM	AS	ASM	AS
<5	9.0 ± 0.3	8.1 ± 0.6	4.78 ± 0.15	3.84 ± 0.19
15	11.3 ± 0.5	8.8 ± 0.3	5.60 ± 0.76	4.17 ± 0.41
30	14.2 ± 0.4	11.1 ± 0.4	5.97 ± 0.56	4.40 ± 0.40
45	18.0 ± 0.7	16.4 ± 0.5	6.18 ± 0.69	4.45 ± 0.38
60	27.0 ± 1.1	24.1 ± 0.5	6.49 ± 0.32	5.42 ± 0.25
75	53.2 ± 0.4	43.5 ± 0.5	7.41 ± 0.21	6.10 ± 0.09
97	790 ± 4	780 ± 6	14.83 ± 0.79	14.53 ± 0.36

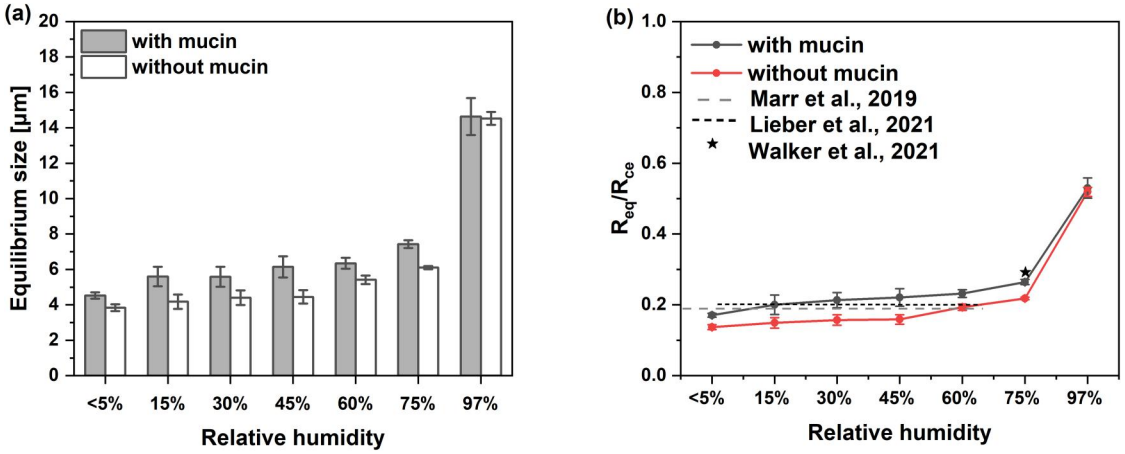

Figure 2. (a) Comparison of the equilibrium radius of saliva droplets with and without mucin at different RH levels. (b) Ratio of equilibrium radius to (stock solution) concentration-equivalent radius (R_{eq}/R_{ce}) as a function of RH for saliva droplets with and without mucin.

range of 0.17 – 0.23 for ASM droplets and within the range of 0.14 – 0.19 for AS droplets. Comparing with low RH measurements, a minor growth in size is evident at 75% RH, reaching 0.27 and 0.22 of their concentration-equivalent sizes for ASM and AS droplets, respectively. At 97% RH, substantially larger equilibrium sizes are observed, these ratios are 0.53 and 0.52, respectively. Marr et al. (2019) predicted that the droplets composed of NaCl and protein would be stable at 0.19 of the initial sizes for RH lower than 64%. Building upon this prediction, Lieber et al. (2021) investigated saliva droplets of various sizes in an acoustic levitator and observed reduction of 0.2 of the initial sizes, irrespective of temperature (ranging from 20 °C to 29 °C) and RH (between 6% and 65%). It is noteworthy that Walker et al. (2021) conducted measurements using the same compositions of artificial saliva solution as utilized in this study, and reported an equilibrium size of 0.29 of the initial size at 75% RH, which is in a good agreement with our results.

In the discussion of the effect of mucin on evaporation kinetics, the comparison of evaporation rates between ASM and AS droplets is of particular interest. For better comparability, we show the evolution of normalized squared droplet diameter (D^2/D_0^2) as a function of time at different RH (Figure 3). This normalization allows for an analysis independent of initial size and a direct phenomenological comparison to the D^2-law characteristic for evaporation of a dilute droplet as known since the beginning of the twentieth

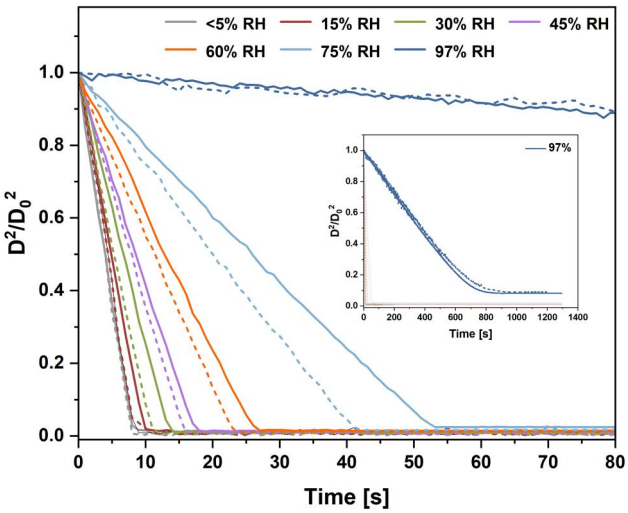

Figure 3. Evolution of normalized surface area of saliva droplets with mucin (solid lines) and without mucin (dashed lines) under different RH conditions. The complete evolution of saliva droplets at 97% is shown in the inset.

century (Langmuir 1918; Wells 1934; Dalla Barba, Wang, and Picano 2021). As shown in Figure 3, the evaporation behavior of ASM and AS droplets both show the linear decrease of surface area (the D^2-law) throughout the evaporation period, with only small deviations observed shortly before equilibrium is reached (Figure S1). A difference in the evaporation kinetics is clearly visible at RH ranging from 15% to 75%, with ASM droplets evaporating slower than AS droplets. This suggests that the presence of mucin hinders the diffusion of water molecules, leading to mass transfer limitations that slow down the evaporation process. However, the role of mucin in evaporation kinetics cannot be unambiguously specified under extremely dry (<5% RH) or extremely humid (97% RH) conditions. We hypothesize that the slow evaporation of the ASM droplets at 97% RH does not result in surface enhancement of mucin concentration which stays evenly distributed across the volume of evaporating droplets, explaining similar evaporation rates of AS and ASM droplets at 97% RH. For the droplets evaporating at very low humidity (<5% RH), the removal of water occurs so fast, that the mucin cannot accumulate at the surface; the whole droplet dries out almost instantaneously, preserving mucin homogeneously distributed across the droplet volume. In this case the evaporation rates are not affected by the mucin surface layer. This explains also the similar morphology for AS and ASM particles extracted from the EDB after drying at <5% RH (see Section 3.2).

Tian et al. (2024) observed only marginal reduction of evaporation rate for artificial saliva droplets containing mucin at 40% RH, but noticed a statistically significant delay of crystallization onset as compared to mucin-free droplets. Based on these observations, they have suggested that mucin would form a viscous "mucin surface film" on evaporating droplets, which affects mass transport and crystallization dynamics.

The experimental data on the content of residual water in evaporating saliva droplets is scarce (Lieber et al. 2021). In this study, we calculate the amount of retained water by subtracting the theoretical weight of dry material based on the initial concentration and saliva composition table (Table 1) from the final weight of saliva droplets which was calculated from recorded light scattering patterns. This calculation assumes a density of 1.002 g/cm^3 for saliva droplets in the original liquid state, 1.24 g/cm^3 (AS) and 1.38 g/cm^3 (ASM) in the solid state (Zhang 2011). The density of the solute droplets during evaporation is calculated with the SADKAT model (Hardy et al. 2023) assuming mass fraction of solute (MFS) = 0.0007 for AS and MFS = 0.0013 for ASM droplets at injection (see SI Table S2). Figure 4 summarizes the amount of water retained within saliva droplets at their equilibrium. Each result is based on the analysis of ten saliva droplets and shows the average as well as the range of values observed. At RH <5%, less than 10 w% of water is retained within saliva droplets after evaporation. At 15% to 45% RH, there is a noticeable increase in the residual water content within ASM droplets. In contrast, AS droplets retain less residual water in this RH range. This results in a noticeable difference in the residual water content between the two types of droplets, particularly at 45% RH, where the difference in the residual weight fraction of water between droplets with and without mucin is on the order of 20 w%. This suggests that the presence of mucin within saliva droplets promotes water retention throughout the evaporation process at intermediate RH. This effect is primarily due to the mucin's hydrophilic nature, which allows it to form hydrogen bonds with water molecules (Ushida and Murata 2013), and its ability to form a semi-permeable layer on the droplet surface (discussed in more detail in Section 3.2). At 60% RH, a significant increase in the residual water content is observed in AS droplets, with the residual weight fraction of water increasing from 15 w% (at 45% RH) to 50 w%, which is comparable to that of ASM droplets. The significant difference in the residual water content within AS droplets between 45% RH and 60% RH indicates that saliva droplets without mucin undergo efflorescence during evaporation in this humidity range. When the RH is below 45%, most of the water in the droplets evaporates due to the absence of mucin. The substantial variability of the residual

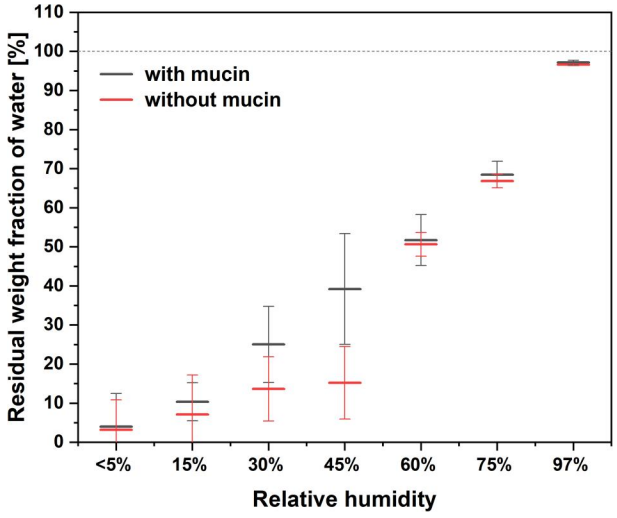

Figure 4. Residual weight fraction of water within saliva droplets at their equilibrium state under different RH conditions.

water fraction at low and intermediate RH below 60% (the observed data range is reflected by the error bars) can be attributed to the sensitivity of the measurements, where even a slight difference in measured radius, as small as 0.1 µm, results in a 5.5% variation in the residual water fraction. The residual weight fraction of water within both types of saliva droplets is comparable under humid conditions, approximately 67 w% and 97 w% at 75% RH and 97% RH.

Regardless of the presence of mucin, elevated virus infectivity under humid conditions, a phenomenon reported in numerous studies (Yang, Elankumaran, and Marr 2012; Prussin et al. 2018; Lin, Schulte, and Marr 2020; Lin and Marr 2020), can be attributed to the following two factors: (1) enhanced water retention within droplets at higher RH, and (2) the formation of virus aggregates during the slower evaporation process at humid conditions, which is expected to enhance virus protection against inactivation as reported by Lin, Schulte, and Marr (2020). Our measurements show that for RH between 30% and 45% a virus would have lower chances to be deactivated due to dehydration in the ASM droplets compared to the mucin-free analogues, as these droplets retain more water in this RH range.

3.2. Morphology of saliva droplets extracted from the EDB

To study the morphology of artificial saliva droplets, we collected droplets from the EDB after they have reached equilibrium size and examined these droplets using SEM. The results are shown in Figure 5. It is important to note that during the transfer and investigation in the SEM, the collected droplets are exposed to very dry conditions, which prevents them from being preserved in their equilibrium state. However, the morphology of collected droplets observed in the SEM reflects their phase state at the moment of deposition on the Si-substrate. The droplets deposited in a liquid state have a flat "pancake" shape and are surrounded by a dark area corresponding to the footprint of a liquid droplet upon deposition. Particles, deposited in a solid or semi-solid state have a compact shape. Example SEM images and details are provided in the SI Figures S2–S4. This apparent difference

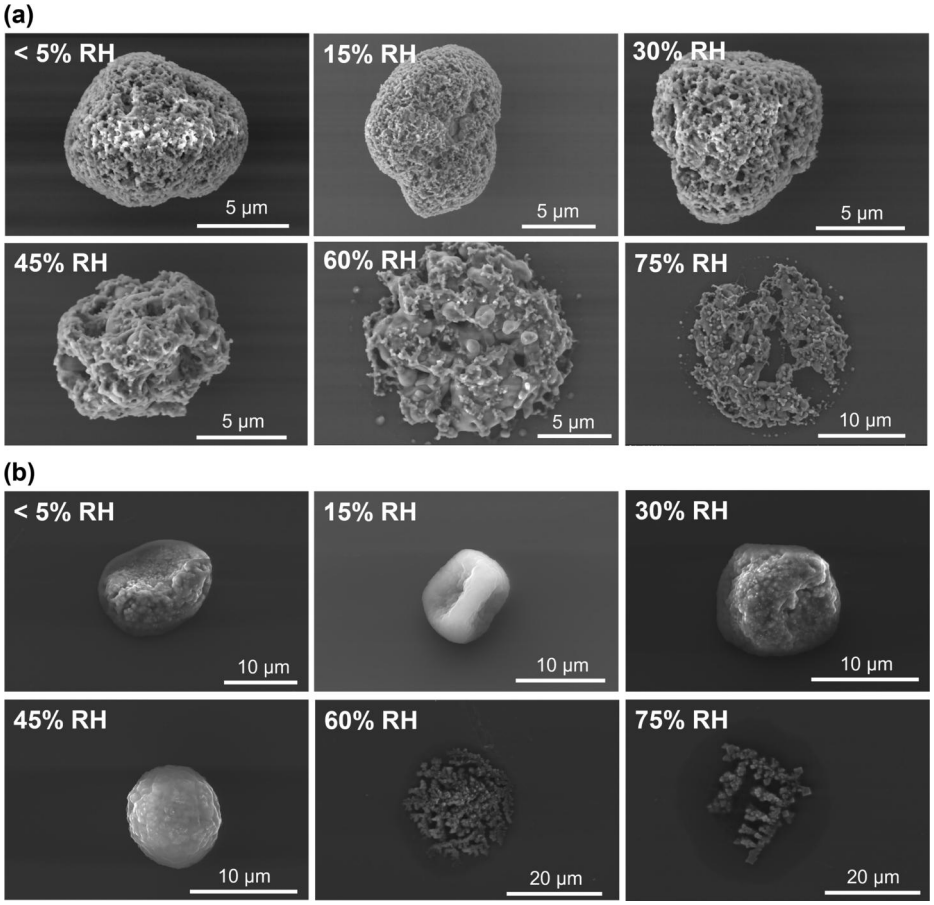

Figure 5. SEM images of saliva droplets collected from the EDB after they reached the equilibrium state under different RH conditions. (a) SEM images of saliva droplets without mucin. (b) SEM images of saliva droplets with mucin.

allows us to deduce the humidity where the transition between the liquid and the semi-solid particle state is taking place while the droplet is suspended in the trap.

Figure 5a shows representative SEM images of AS droplets. The droplets transition to a solid or semi-solid state at RH $\leq$ 45%, whereas they remain in a liquid state at higher RH. This observation corroborates the findings on the residual weight fraction of water within AS droplets discussed in Section 3.1: (1) AS droplets remain in a liquid state at RH of 60% or higher. (2) At RH of 45% or lower, most of the water in AS droplets has evaporated, as evidenced by the formation of crystalline material in a compact solid or semi-solid state. This is close to the RH for efflorescence of NaCl of 45–48% (Ahn et al. 2010; Li et al. 2014). Similar SEM images are shown in Tian et al. (2024), who collected mucin-free saliva particles falling and drying in a tube at 40% RH. Additional SEM images for AS droplets are shown in SI Figure S5.

Importantly, the presence of mucin leads to more pronounced morphological variations in artificial saliva droplet residues, as shown in Figure 5b. ASM droplets assume an amorphous-like morphology already at RH $\leq$ 45% and do not exhibit a porous structure, unlike AS residues under dry conditions. Instead, the crystalline material appears to be covered by a layer of organic material (element quantification see SI Table S3). The distinct morphology differences observed at RH $\leq$ 45% between ASM and AS droplets are attributable to the presence of mucin, which is the sole difference in the formulation of the two saliva solutions. Our observations go in line with the previous study of Huynh et al. (2022), who reported that a higher protein content results in formation of a protein-enriched shell across a range of RH. More SEM images for ASM droplets are shown in SI Figure S6.

In addition, considering the various industrial applications of artificial saliva, we tested an additional type of artificial salvia solution that resembles the mineral composition of natural saliva, lacking mucin but high in urea, and find that urea behaves similarly to mucin during droplet evaporation, creating a compact layer covering inorganic salt crystals (see SI Figure S7).

In Figure 5b, RH demonstrates a notable effect on the extent of shape depression observed on the semi-solid organic layer at RH levels of 45% and below. Most semi-solid configurations showing pronounced depressions occur at RH levels of 30% or lower, where rapid increase in viscosity coincides with the development of surface depressions. The viscous layer remains permeable to water molecules, as shown by the decreasing residual water content at lower RH. Due to its viscous nature, this layer cannot readily adjust to the shrinking central part of the droplet, ultimately causing its collapse. The influence of mucin on the droplet shape will be further discussed in Section 3.4.

Previous studies have suggested that the efflorescence of inorganic salts helps virus to survive in the droplets by reducing the concentration of electrolytes (Huynh et al. 2022; Niazi et al. 2021b; Tian et al. 2024). However, the presence of mucin in saliva droplets cannot be ignored. Alexander et al. (2022) investigated the infectivity of the virus in droplets with varying mucin concentrations at 40% RH, reporting that the mean infectivity of virus in droplets containing 0.1% *w/v* mucin is approximately 20% higher than that in droplets without mucin, and the infectivity become stronger with an increasing mucin content within droplets. Zuo et al. (2014) also observed a notable enhancement in the infectivity and survival of airborne MS2 bacteriophage in aerosolized ASM compared to AS, at a (45% ± 5%) RH and a temperature of 22 °C to 24 °C. The infectious virus to total virus ratio (ITR) is significantly higher, measuring 0.527 with mucin compared to 0.114 without mucin. Lin and Marr (2020) reported that viruses in suspended aerosols can keep their infectivity under extremely dry conditions, with little to no decay of infectivity at RH below 33%, but with reduced infectivity at intermediate RH (from 40% to 60%). Based on our observations, we propose an additional factor that may explain the survival of the viruses under extremely dry conditions: the surface layer of saliva droplets, enriched with mucin, protects viruses from inactivation by retaining water from evaporation. Enveloped viruses, such as coronaviruses, are more sensitive to environmental changes compared to non-enveloped viruses (Zeng et al. 2023). The hydrophobic nature of the viral envelope may cause them to remain within the droplet rather than go to the droplet surface (Vejerano and Marr 2018; Huynh et al. 2022). Thus, the mucin-rich viscous layer can act as a physical barrier, potentially limiting the exposure of viruses to environmental conditions.

3.3. Hygroscopic growth of levitated saliva droplets

Water uptake controls the size, phase state, and chemical properties of saliva droplets (Jing et al. 2017). Respiratory aerosol particles exhibiting strong hygroscopic growth would be more rapidly removed by

sedimentation, consequently contributing less to the transmission of pathogens. The highly hygroscopic compounds, such as KCl and NaCl, contribute almost 1/3 of the weight of the soluble material in artificial saliva. NaCl has a high degree of hygroscopicity, with a hygroscopic growth factor of 2.38 measured for 100 nm NaCl particles at 90% RH (Zieger et al. 2017) and the hygroscopic growth factor measured for 100 nm KCl particles is 2.05 at the same RH (Jing et al. 2017). However, organic aerosols are reported to have a low hygroscopic growth factor, with a value < 0.05 (Groth et al. 2021; Walker et al. 2021). Given the chemical complexity of saliva droplets, the hygroscopic behavior of concentrated saliva droplets cannot be predicted from hygroscopic behavior of individual components. Understanding how saliva droplets respond to the change of the ambient RH is crucial for predicting the airborne transmission of pathogens.

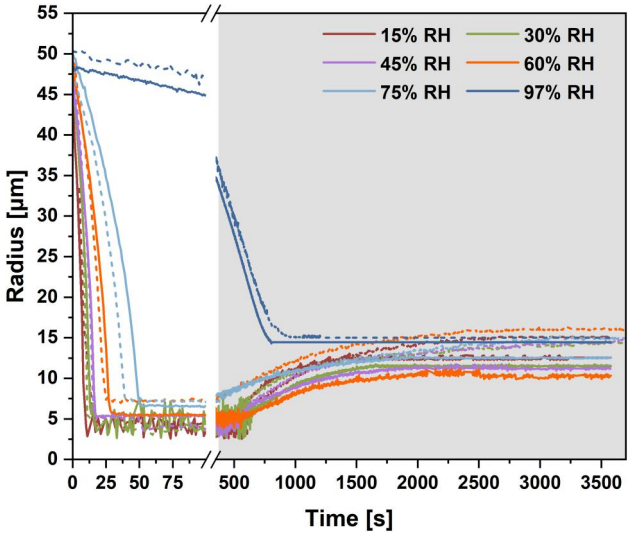

Figure 6. Evaporation and hygroscopic growth of representative saliva droplets with mucin (solid lines) and without mucin (dashed lines). The grey area in the figure indicates the rehydration stage at 97% RH.

To assess the hygroscopicity of the saliva droplets dried at various RH, we have measured the hygroscopic growth of these droplets exposed to 97% RH. The results are presented in Figure 6 (Figure S8 shows the data of Figure 6 separately). For hygroscopic growth measurements, saliva droplets were levitated at equilibrium for 5 min at a specific constant RH. Then, the RH was increased in a single step to 97% RH. While the RH in the human mouth is typically assumed to be 99.5% (Morawska et al. 2009), it was set at a maximum of 97% RH in our study to ensure a proper operation of the EDB. After the humidity inside the EDB reached 97% RH, a process taking approximately 3 to 10 min depending on the initial RH, the droplets were kept suspended in the gas flow for one hour.

Figure 7a shows the ratio of droplet radius upon reaching equilibrium at rehydration and droplet initial radius. The weight fraction of water within saliva droplets after rehydration at 97% RH is shown in Figure 7b. For comparison, the size and water fraction of ASM and AS droplets injected into the EDB and kept at 97% RH are represented by grey and red bands in both figures.

For AS droplets, the hygroscopic growth at 97% RH remains unaffected by the evaporation process under different RH conditions. All size ratios revert to

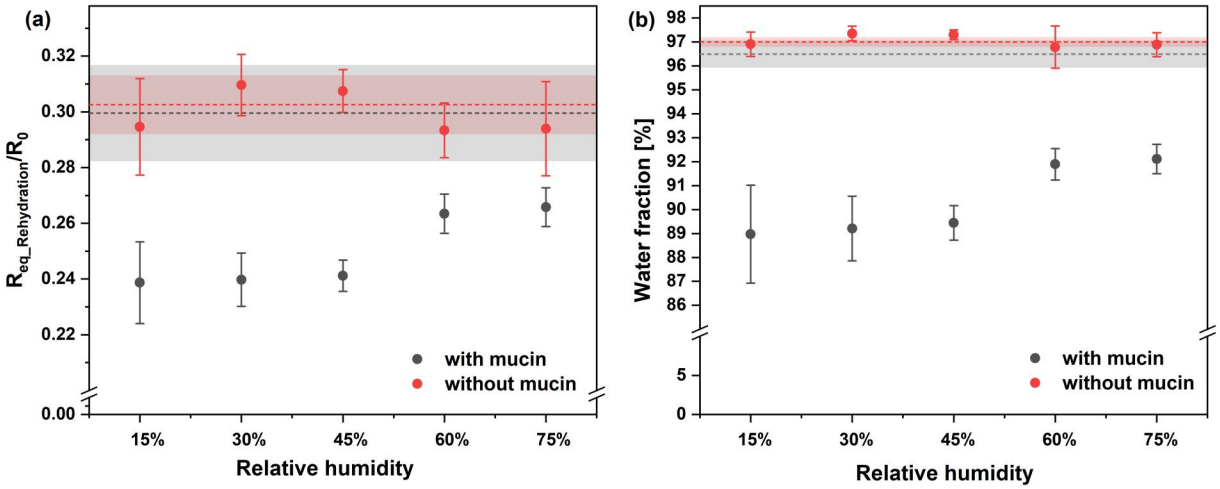

Figure 7. Relative change of the saliva droplet size and water uptake upon rehydration at RH = 97%. The RH on the x-axis gives the equilibrium RH prior to rehydration. (a) Ratio of the equilibrium size following rehydration ($R_{eq\_Rehydration}$) to the initial droplet size as a function of the RH at which saliva droplets initially underwent evaporation. The dashed lines indicate the average ratio of saliva droplets that evaporated at 97%, with the shaded area showing the standard deviation. (b) Water fraction of saliva droplets with and without mucin after achieving the equilibrium at rehydration. The dashed lines indicate the reference at 97% RH.

the reference interval (0.303 ± 0.01), and the water content of the rehydrated saliva droplets reaches as high as 97 w%, consistent with the water content in the reference droplets. However, ASM droplets are less hygroscopic. The size recovery of ASM droplets during rehydration at 97% RH is incomplete. The size ratio decreases to (0.241 ± 0.009) and the water content falls to less than 90 w% when droplets initially evaporate under dry conditions (RH $\leq$ 45%). In comparison, the reference size ratio is (0.299 ± 0.017), with a reference water fraction of 96.5 w%. However, the hygroscopicity of evaporated ASM droplets under 60% and 75% RH conditions is slightly higher. The size ratio increases to (0.260 ± 0.006), and the water content within the droplets correspondingly rises to 92 w%.

The difference in the hygroscopicity between ASM droplets and AS droplets implies that the presence of mucin retards the water uptake process, even at humidity where the droplets preserve their apparent liquid or semi-liquid state. As discussed in Section 3.2 (Figure 5), SEM images of saliva droplets collected from EDB provide a more detailed insight into the underlying factors contributing to the disparities in hygroscopic properties. When RH $\leq$ 45%, the mucin forms a layer on the surface of saliva droplets, covering salt crystals. This layer hinders the water uptake by saliva droplets with mucin. Even at high RH, the ASM droplets do not recover their sizes compared to AS saliva droplets. This observation suggests that the presence and the state of mucin are influential factors contributing to the limitation observed in the hygroscopic growth of saliva droplets. Our results align closely with a previous study by Choi and Chan (2002), who reported that organic components exert a strong influence on the hygroscopic behavior of inorganic components and the growth factors of droplets containing inorganic and organic mixtures are lower than those of the pure inorganic species.

3.4. Light scattering patterns of levitated saliva droplets

To further elucidate how the presence of mucin influences the evaporation and hygroscopic growth of saliva droplets, we now discuss the morphology of levitated saliva droplets based on their light scattering patterns. In Figure 8, we compare the light scattering patterns of an AS droplet (Figure 8a) and an ASM droplet (Figure 8b) under changing RH conditions. At the beginning, a saliva droplet was trapped at 97% RH and levitated for 10 min. Then, RH was decreased step by step from 97% to 25%, all while the saliva droplet remained stably levitated. After reaching 25% RH, the RH was adjusted back to 97% in one step and the light scattering patterns were continuously recorded while the droplet remained stably levitated under these conditions.

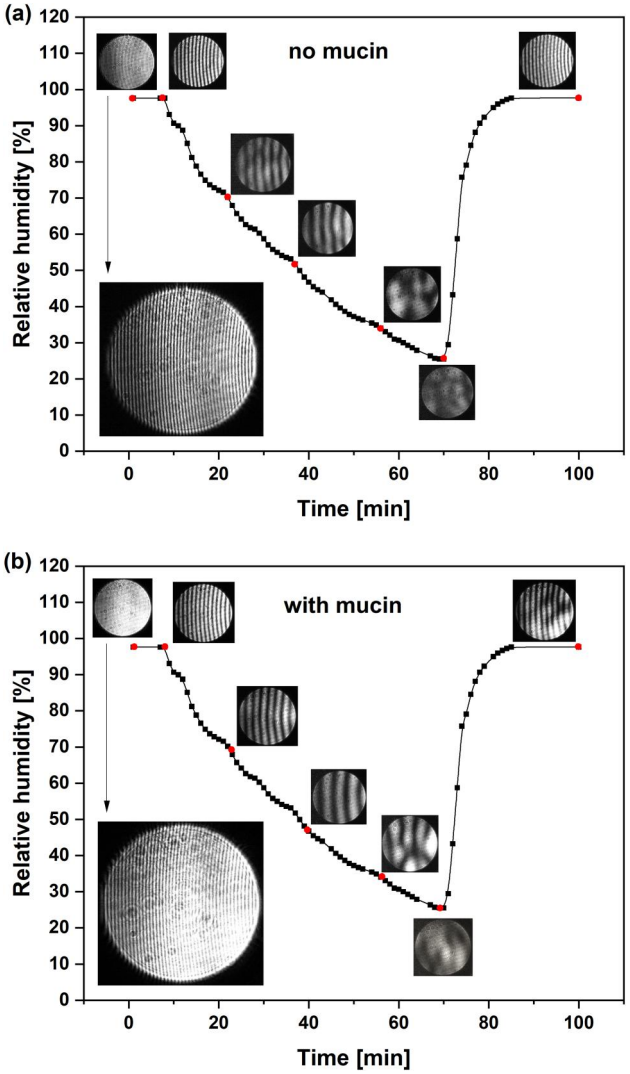

Figure 8. Series of light scattering patterns of saliva droplets with changing RH: (a) A representative saliva droplet without mucin. (b) A representative saliva droplet with mucin. The red dots indicate time and RH at which the light scattering patterns were recorded. An enlarged version of the initial light scattering patterns of both droplets is shown in the lower left corner of the graph for clarity.

In Figure 8a, for the AS droplet, with decreasing RH, the diminishing number of vertical stripes in the light scattering patterns reflects a reduction in droplet size. A noticeable distortion of the scattering pattern is observed after the RH drops down to 70% (Figure S9), suggesting onset of crystallization within the levitated droplet and a loss of its original spherical shape.

As evaporation proceeds, the number of stripes in the scattering patterns reduces and the stripes become increasingly irregular. A distinct increase in the number of stripes on the light scattering patterns could be observed following humidification.

The ASM droplet (Figure 8b) preserves its spherical shape for a longer time compared with the AS droplet, as indicated by the stripes remaining regular until the RH drops below 45%. At this point, the scattering patterns become irregular. This suggests that the droplet undergoes significant changes in morphology, possibly deviating from its spherical shape. This conclusion is consistent with the observation that saliva particles become non-spherical at RH below 50% (Walker et al. 2021).

Upon comparing the light scattering patterns of the two types of saliva droplets, it becomes evident that the onset of pattern distortion in mucin-containing droplets is noticeably delayed in comparison to mucin-free droplets. This observation suggests that the presence of mucin contributes to the prolonged preservation of a spherical shape of the saliva droplet. This effect is likely due to the specific properties of mucin, such as viscoelasticity and surface activity: (1) Viscoelastic properties of mucin (McCullagh et al. 1995) may allow droplets to retain their spherical shape during evaporation through its ability to resist deformation for a more extended period. (2) Mucin can affect the surface tension of the saliva droplets (Mikos and Peppas 1989). By altering the surface tension, mucin may influence the tendency for droplet to deform during evaporation. This could also contribute to the spherical shape being preserved for a longer time.

4. Conclusions

This study investigated the role of mucin in saliva droplets from two aspects: (1) evaporation process and hygroscopic growth of levitated artificial saliva droplets in an EDB; (2) the evolution of microphysical structure and morphology of artificial saliva droplet using light scattering patterns and SEM, in order to extend the understanding of the RH-dependent infectivity of viruses loaded in saliva droplets. The presence of mucin influences both evaporation kinetics and equilibrium thermodynamics of artificial saliva droplets, which cannot be explained by the presence as an additional soluble component alone. We hypothesize, that it facilitates the formation of a semi-permeable viscous layer on the surface of saliva droplets during evaporation under low-to-moderate humidity conditions ($5 < \mathrm{RH} \leq 45\%$). This mucin-rich surface layer reduces the water evaporation rate and retains a small extra fraction of water within the saliva droplets, thereby maintaining a favorable environment for viruses and other pathogens. Additionally, mucin hinders water uptake during rehydration, leading to reduced hygroscopic growth and, consequently, smaller droplet sizes. Respiratory particles that form a semi-solid organic surface layer before contacting a solid surface would be more readily resuspended by everyday human activity or through advection by air currents. Reduced hygroscopic growth of saliva droplets upon repeated inhalation would facilitate deeper penetration of virus-laden particles into the human respiratory tract thus increasing potential infections to the lungs.

Our observations suggest that the possible formation of a mucin-enriched layer may contribute to explaining the RH-dependent infectivity of viruses. Other proteins and organic substances present in the respiratory fluids may have the potential to generate virus-laden respiratory droplets and form even more robust organic shell under dry conditions, thereby enhancing the transmissivity of viruses by shielding them from influences of environmental factors such as temperature, humidity, and UV radiation. This topic should be a subject of further research.

Acknowledgments

We would like to acknowledge Dr. J. P. Reid and Dr. J. Tian, University of Bristol, for the helpful discussions and assistance in using the SADKAT model, and Dr. S. H. Jones, KIT, for her support.

Disclosure statement

No potential conflict of interest was reported by the author(s).

Funding

This work was supported by Helmholtz Association of German Research Centers (HGF) under the CORAERO project (KA1-Co-06). YM acknowledges the financial support from KHYS-Networking grant, KIT.

ORCID

Yue Meng http://orcid.org/0009-0006-3259-4837
Alexei Kiselev http://orcid.org/0000-0003-0136-2428
Denis Duft http://orcid.org/0000-0003-2943-3574
Thomas Dresch http://orcid.org/0000-0002-5753-9010
Thomas Leisner http://orcid.org/0000-0001-9693-7671

References

Ahlawat, A., A. Wiedensohler, and S. K. Mishra. 2020. An overview on the role of relative humidity in airborne transmission of SARS-CoV-2 in indoor environments. *Aerosol Air Qual. Res.* 20 (9):1856–61. doi: 10.4209/aaqr.2020.06.0302.

Ahn, K. H., S. M. Kim, H. J. Jung, M. J. Lee, H. J. Eom, S. Maskey, and C. U. Ro. 2010. Combined use of optical and electron microscopic techniques for the measurement of hygroscopic property, chemical composition, and morphology of individual aerosol particles. *Anal. Chem.* 82 (19):7999–8009. doi: 10.1021/ac101432y.

Alexander, R. W., J. Tian, A. E. Haddrell, H. P. Oswin, E. Neal, D. A. Hardy, M. Otero-Fernandez, J. F. S. Mann, T. A. Cogan, A. Finn, et al. 2022. Mucin transiently sustains coronavirus infectivity through heterogenous changes in phase morphology of evaporating aerosol. *Viruses* 14 (9):1856. doi: 10.3390/v14091856.

Ali, M., E. P. Lillehoj, Y. Park, Y. Kyo, and K. C. Kim. 2011. Analysis of the proteome of human airway epithelial secretions. *Proteome Sci.* 9 (1):4. doi: 10.1186/1477-5956-9-4.

Baliga, S., S. Muglikar, and R. Kale. 2013. Salivary pH: A diagnostic biomarker. *J. Indian Soc. Periodontol.* 17 (4):461–5. doi: 10.4103/0972-124X.118317.

Boat, T. F., and P. W. Cheng. 1980. Biochemistry of airway mucus secretions. *Fed. Proc.* 39 (13):3067–74. PMID: 7428951.

Chen, X., X. Zhou, X. Xia, X. Xie, P. Lu, and Y. Feng. 2021. Modeling of the transport, hygroscopic growth, and deposition of multi-component droplets in a simplified airway with realistic thermal boundary conditions. *J. Aerosol Sci.* 151:105626. doi: 10.1016/j.jaerosci.2020.105626.

Choi, M. Y., and C. K. Chan. 2002. The effects of organic species on the hygroscopic behaviors of inorganic aerosols. *Environ. Sci. Technol.* 36 (11):2422–8. doi: 10.1021/es0113293.

Corfield, A. P. 2015. Mucins: A biologically relevant glycan barrier in mucosal protection. *Biochim. Biophys. Acta.* 1850 (1):236–52. doi: 10.1016/j.bbagen.2014.05.003.

Dalla Barba, F., J. Wang, and F. Picano. 2021. Revisiting D^2-law for the evaporation of dilute droplets. *Phys. Fluids* 33 (5):051701. doi: 10.1063/5.0051078.

Ebert, M., S. Weinbruch, A. Rausch, G. Gorzawski, G. Helas, P. Hoffmann, and H. Wex. 2002. Complex refractive index of aerosols during LACE 98 as derived from the analysis of individual particles. *J. Geophys. Res.* 107 (D21):8121. doi: 10.1029/2000JD000195.

Groth, R., L. T. Cravigan, S. Niazi, Z. Ristovski, and G. R. Johnson. 2021. *In situ* measurements of human cough aerosol hygroscopicity. *J. R Soc. Interface* 18 (178):20210209. doi: 10.1098/rsif.2021.0209.

Guo, L., Z. Yang, L. Zhang, S. Wang, T. Bai, Y. Xiang, and E. Long. 2021. Systematic review of the effects of environmental factors on virus inactivation: Implications for coronavirus disease 2019. *Int. J. Environ. Sci. Technol. (Tehran)* 18 (9):2865–78. doi: 10.1007/s13762-021-03495-9.

Haddrell, A., M. Otero-Fernandez, H. Oswin, T. Cogan, J. Bazire, J. Tian, R. Alexander, J. F. S. Mann, D. Hill, A. Finn, et al. 2023. Differences in airborne stability of SARS-CoV-2 variants of concern is impacted by alkalinity of surrogates of respiratory aerosol. *J. R Soc. Interface* 20 (203):20230062. doi: 10.1098/rsif.2023.0062.

Hardy, D. A., J. F. Robinson, T. G. Hilditch, E. Neal, P. Lemaitre, J. S. Walker, and J. P. Reid. 2023. Accurate measurements and simulations of the evaporation and trajectories of individual solution droplets. *J. Phys. Chem. B* 127 (15):3416–30. doi: 10.1021/acs.jpcb.2c08909.

Hoffmann, N., A. Kiselev, D. Rzesanke, D. Duft, and T. Leisner. 2013. Experimental quantification of contact freezing in an electrodynamic balance. *Atmos. Meas. Tech.* 6 (9):2373–82. doi: 10.5194/amt-6-2373-2013.

Huynh, E., A. Olinger, D. Woolley, R. K. Kohli, J. M. Choczynski, J. F. Davies, K. Lin, L. C. Marr, and R. D. Davis. 2022. Evidence for a semisolid phase state of aerosols and droplets relevant to the airborne and surface survival of pathogens. *Proc. Natl. Acad. Sci. USA*. 119 (4):e2109750119. doi: 10.1073/pnas.2109750119.

Jing, B., C. Peng, Y. Wang, Q. Liu, S. Tong, Y. Zhang, and M. Ge. 2017. Hygroscopic properties of potassium chloride and its internal mixtures with organic compounds relevant to biomass burning aerosol particles. *Sci. Rep.* 7 (1):43572. doi: 10.1038/srep43572.

Kudo, E., E. Song, L. J. Yockey, T. Rakib, P. W. Wong, R. J. Homer, and A. Iwasaki. 2019. Low ambient humidity impairs barrier function and innate resistance against influenza infection. *Proc. Natl. Acad. Sci. U S A* 116 (22):10905–10. doi: 10.1073/pnas.1902840116.

Langmuir, I. 1918. The evaporation of small spheres. *Phys. Rev.* 12:368–70. doi: 10.1103/PhysRev.12.368.

Lewis, D. 2022. Why the WHO took two years to say COVID is airborne. *Nature* 604 (7904):26–31. doi: 10.1038/d41586-022-00925-7.

Li, X., D. Gupta, H. J. Eom, H. Kim, and C. U. Ro. 2014. Deliquescence and efflorescence behavior of individual NaCl and KCl mixture aerosol particles. *Atmos. Environ.* 82:36–43. doi: 10.1016/j.atmosenv.2013.10.011.

Lieber, C., S. Melekidis, R. Koch, and H. J. Bauer. 2021. Insights into the evaporation characteristics of saliva droplets and aerosols: Levitation experiments and numerical modeling. *J. Aerosol Sci.* 154:105760. doi: 10.1016/j.jaerosci.2021.105760.

Lin, K., and L. C. Marr. 2020. Humidity-dependent decay of viruses, but not bacteria, in aerosols and droplets follows disinfection kinetics. *Environ. Sci. Technol.* 54 (2):1024–32. doi: 10.1021/acs.est.9b04959.

Lin, K., C. R. Schulte, and L. C. Marr. 2020. Survival of MS2 and Φ6 viruses in droplets as a function of relative humidity, pH, and salt, protein, and surfactant concentrations. *PLoS One.* 15 (12):e0243505. doi: 10.1371/journal.pone.0243505.

Liu, L., J. Wei, Y. Li, and A. Ooi. 2017. Evaporation and dispersion of respiratory droplets from coughing. *Indoor Air.* 27 (1):179–90. doi: 10.1111/ina.12297.

Luo, B., A. Schaub, I. Glas, L. K. Klein, S. C. David, N. Bluvshtein, K. Violaki, G. Motos, M. O. Pohl, W. Hugentobler, et al. 2023. Acidity of expiratory aerosols controls the infectivity of airborne influenza virus and SARS-CoV-2. *Environ. Sci. Technol.* 57 (1):486–97. doi: 10.1021/acs.est.2c05777.

Marr, L. C., J. W. Tang, J. Van Mullekom, and S. S. Lakdawala. 2019. Mechanistic insights into the effect of

humidity on airborne influenza virus survival, transmission and incidence. *J. R Soc. Interface* 16 (150):20180298. doi: 10.1098/rsif.2018.0298.

McCullagh, C. M., A. M. Jamieson, J. Blackwell, and R. Gupta. 1995. Viscoelastic properties of human tracheobronchial mucin in aqueous solution. *Biopolymers* 35 (2): 149–59. doi: 10.1002/bip.360350203.

Mikos, A. G., and N. A. Peppas. 1989. Measurement of the surface tension of mucin solutions. *Int. J. Pharm.* 53 (1): 1–5. doi: 10.1016/0378-5173(89)90354-2.

Morawska, L., and J. Cao. 2020. Airborne transmission of SARS-CoV-2: The world should face the reality. *Environ. Int.* 139:105730. doi: 10.1016/j.envint.2020.105730.

Morawska, L., G. R. Johnson, Z. D. Ristovski, M. Hargreaves, K. Mengersen, S. Corbett, C. Y. H. Chao, Y. Li, and D. Katoshevski. 2009. Size distribution and sites of origin of droplets expelled from the human respiratory tract during expiratory activities. *J. Aerosol Sci.* 40 (3): 256–69. doi: 10.1016/j.jaerosci.2008.11.002.

Niazi, S., R. Groth, L. Cravigan, C. He, J. W. Tang, K. Spann, and G. R. Johnson. 2021b. Susceptibility of an airborne common cold virus to relative humidity. *Environ. Sci. Technol.* 55 (1):499–508. doi: 10.1021/acs.est.0c06197.

Niazi, S., K. R. Short, R. Groth, L. Cravigan, K. Spann, Z. Ristovski, and G. R. Johnson. 2021a. Humidity-dependent survival of an airborne influenza A virus: Practical implications for controlling airborne viruses. *Environ. Sci. Technol. Lett.* 8 (5):412–8. doi: 10.1021/acs.estlett.1c00253.

Nikfar, M., R. Paul, K. Islam, M. Razizadeh, A. Jagota, and Y. Liu. 2021. Respiratory droplet resuspension near surfaces: Modeling and analysis. *J. Appl. Phys.* 130 (2):024702. doi: 10.1063/5.0050447.

Oswin, H. P., A. E. Haddrell, M. Otero-Fernandez, J. F. S. Mann, T. A. Cogan, T. G. Hilditch, J. Tian, D. A. Hardy, D. J. Hill, A. Finn, et al. 2022. The dynamics of SARS-CoV-2 infectivity with changes in aerosol microenvironment. *Proc. Natl. Acad. Sci. U S A* 119 (27):e2200109119. doi: 10.1073/pnas.2200109119.

Parienta, D., L. Morawska, G. R. Johnson, Z. D. Ristovski, M. Hargreaves, K. Mengersen, S. Corbett, C. Y. H. Chao, Y. Li, and D. Katoshevski. 2011. Theoretical analysis of the motion and evaporation of exhaled respiratory droplets of mixed composition. *J. Aerosol Sci.* 42 (1):1–10. doi: 10.1016/j.jaerosci.2010.10.005.

Prather, K. A., C. C. Wang, and R. T. Schooley. 2020. Reducing transmission of SARS-CoV-2. *Science* 368 (6498):1422–4. doi: 10.1126/science.abc6197.

Prussin, A. J., D. O. Schwake, K. Lin, D. L. Gallagher, L. Buttling, and L. C. Marr. 2018. Survival of the enveloped virus Phi6 in droplets as a function of relative humidity, absolute humidity, and temperature. *Appl. Environ. Microbiol.* 84 (12):e00551-18. doi: 10.1128/AEM.00551-18.

Rzesanke, D., J. Nadolny, D. Duft, R. Müller, A. Kiselev, and T. Leisner. 2012. On the role of surface charges for homogeneous freezing of supercooled water microdroplets. *Phys. Chem. Chem. Phys.* 14 (26):9359–63. doi: 10.1039/c2cp23653b.

Schuit, M., S. Ratnesar-Shumate, J. Yolitz, G. Williams, W. Weaver, B. Green, D. Miller, M. Krause, K. Beck, S. Wood, et al. 2020. Airborne SARS-CoV-2 is rapidly inactivated by simulated sunlight. *J. Infect. Dis.* 222 (4): 564–71. doi: 10.1093/infdis/jiaa334.

Singh, M., S. H. Jones, A. Kiselev, D. Duft, and T. Leisner. 2023. The viscosity and surface tension of supercooled levitated droplets determined by excitation of shape oscillations. *Atmos. Meas. Tech.* 16 (21):5205–15. doi: 10.5194/amt-16-5205-2023.

Smither, S. J., L. S. Eastaugh, J. S. Findlay, and M. S. Lever. 2020. Experimental aerosol survival of SARS-CoV-2 in artificial saliva and tissue culture media at medium and high humidity. *Emerg. Microbes Infect.* 9 (1):1415–7. doi: 10.1080/22221751.2020.1777906.

Stewart, D. J., C. Cai, J. Nayler, T. C. Preston, J. P. Reid, U. K. Krieger, C. Marcolli, and Y. H. Zhang. 2015. Liquid-liquid phase separation in mixed organic/inorganic single aqueous aerosol droplets. *J. Phys. Chem. A* 119 (18):4177–90. doi: 10.1021/acs.jpca.5b01658.

Takehara, S., M. Yanagishita, K. A. Podyma-Inoue, and Y. Kawaguchi. 2013. Degradation of MUC7 and MUC5B in human saliva. *PLoS One.* 8 (7):e69059. doi: 10.1371/journal.pone.0069059.

Tang, J. W., W. P. Bahnfleth, P. M. Bluyssen, G. Buonanno, J. L. Jimenez, J. Kurnitski, Y. Li, S. Miller, C. Sekhar, L. Morawska, et al. 2021. Dismantling myths on the airborne transmission of severe acute respiratory syndrome coronavirus-2 (SARS-CoV-2). *J. Hosp. Infect.* 110:89–96. doi: 10.1016/j.jhin.2020.12.022.

Tian, J., R. W. Alexander, D. A. Hardy, T. G. Hilditch, H. P. Oswin, A. E. Haddrell, and J. P. Reid. 2024. The microphysics of surrogates of exhaled aerosols from the upper respiratory tract. *Aerosol Sci. Technol.* 58 (4):461–74. doi: 10.1080/02786826.2023.2299214.

Ushida, K., and T. Murata. 2013. Materials science and engineering of mucin. A new aspect of mucin chemistry. *Stud. Nat. Prod. Chem.* 39:115–59. doi: 10.1016/B978-0-444-62615-8.00004-7.

Vejerano, E. P., and L. C. Marr. 2018. Physico-chemical characteristics of evaporating respiratory fluid droplets. *J. R Soc. Interface* 15 (139):20170939. doi: 10.1098/rsif.2017.0939.

Vu, T. V., Z. Shi, and R. M. Harrison. 2021. Estimation of hygroscopic growth properties of source-related submicrometre particle types in a mixed urban aerosol. *NPJ Clim. Atmos. Sci.* 4:21. doi: 10.1038/s41612-021-00175-w.

Walker, J. S., J. Archer, F. K. A. Gregson, S. E. S. Michel, B. R. Bzdek, and J. P. Reid. 2021. Accurate representations of the microphysical processes occurring during the transport of exhaled aerosols and droplets. *ACS Cent. Sci.* 7 (1):200–9. doi: 10.1021/acscentsci.0c01522.

Wang, C. C., K. A. Prather, J. Sznitman, J. L. Jimenez, S. S. Lakdawala, Z. Tufekci, and L. C. Marr. 2021. Airborne transmission of respiratory viruses. *Science* 373 (6558): eabd9149. doi: 10.1126/science.abd9149.

Wells, W. F. 1934. On air-borne infection: Study II. Droplets and droplet nuclei. *Am. J. Epidemiol* 20:611–8. doi: 10.1093/oxfordjournals.aje.a118097.

Yang, W., S. Elankumaran, and L. C. Marr. 2012. Relationship between humidity and influenza A viability in droplets and implications for influenza's seasonality. *PLoS One.* 7 (10): e46789. doi: 10.1371/journal.pone.0046789.

Zeng, L., J. Li, M. Lv, Z. Li, L. Yao, J. Gao, Q. Wu, Z. Wang, X. Yang, G. Tang, et al. 2023. Environmental stability and transmissibility of enveloped viruses at varied

animate and inanimate interfaces. *Environ. Health (Wash)* 1 (1):15–31. doi: 10.1021/envhealth.3c00005.

Zhang, T. 2011. Study on surface tension and evaporation rate of human saliva, saline, and water droplets. Graduate Theses, Dissertations, and Problem Reports 2271. doi: 10.33915/etd.2271.

Zieger, P., O. Väisänen, J. C. Corbin, D. G. Partridge, S. Bastelberger, M. Mousavi-Fard, B. Rosati, M. Gysel, U. K. Krieger, C. Leck, et al. 2017. Revising the hygroscopicity of inorganic sea salt particles. *Nat. Commun.* 8 (1):15883. doi: 10.1038/ncomms15883.

Zuo, Z., T. H. Kuehn, A. Z. Bekele, S. K. Mor, H. Verma, S. M. Goyal, P. C. Raynor, and D. Y. H. Pui. 2014. Survival of airborne MS2 bacteriophage generated from human saliva, artificial saliva, and cell culture medium. *Appl. Environ. Microbiol.* 80 (9):2796–803. doi: 10.1128/AEM.00056-14.